Smart glazing for energy- and cost-efficient greenhouse humidity regulation

*Zijian Weng [a, ‡], Omar Khater [a, ‡], Vladislav Paley [a], Nathan K. Kessenich [b], Logan G. Schmid [c], Marco U. Lam [a], Abhishek Dyade [a], Zengyu Zhan [a], Wenbin Mao [a, *], Long Wang [d, *], and Ying Zhong [e, *]*

[a] Department of Mechanical Engineering, University of South Florida, 4202 E. Fowler Ave, Tampa, FL 33620, USA

[b] Department of Mechanical Engineering, California Polytechnic State University, 1 Grand Ave, San Luis Obispo, CA 93407, USA

[c] Department of Biomedical Engineering, California Polytechnic State University, 1 Grand Ave, San Luis Obispo, CA 93407, USA

[d] Department of Civil and Environmental Engineering, California Polytechnic State University, 1 Grand Ave, San Luis Obispo, CA 93407, USA

[e] Sauvage Laboratory for Smart Materials, School of Integrated Circuit, Harbin Institute of Technology (Shenzhen), University Town of Shenzhen, Shenzhen, Guangdong 518055, China

***Corresponding authors**:

Ying Zhong, zhongy@hit.edu.cn;

Long Wang, lwang38@calpoly.edu; Wenbin Mao, wmao@usf.edu

‡ These authors have the same contribution to the study.

Abstract

Global food shortage demands significant progress in crop production. Greenhouses offer a solution for higher crop production by providing controllable environment. Excess levels of humidity, however, encourages pests and diseases, drastically reducing crop yields. Traditional humidity control methods for greenhouses are expensive and energy intensive. In addition to this, non-biodegradable plastic covers cause massive white pollution. To tackle these concerns, we present to use smart glazing and sensors for greenhouse humidity regulation through both passive and active paths. We created biodegradable humidity-sensitive films by blending polyethylene glycol (PEG) with cellulose acetate (CA). PEG/CA covers can automatically open for air circulation at high humidity, successfully demonstrating repeatable greenhouse humidity regulation to as low as 60% relative humidity. PEG/CA based humidity sensors can actively accelerate air circulation and humidity reduction with repeated cycles at even higher efficiency. Overall, our research introduces a low-cost, all-in-one, sustainable, environmentally conscious, solution for addressing the greenhouse humidity control challenges. Approximately, this solution can potentially achieve annual energy saving up to 56.6 gigawatt-hours for the US if fully applied.

Keywords: Smart greenhouse glazing, polymer blend, humidity sensitive, sustainability, automatic humidity regulation

INTRODUCTION

Globally, there are still over 45 million people suffering from famine or famine-like conditions.[1] Food crisis has been further aggravated by pandemics, conflicts, climate change, and shrinkage of arable land areas.[2–4] There are urgent needs of energy and cost-efficient solutions to promote the yield from farmlands. Because of the precisely controlled climate, increased production, and decreased disease, greenhouse farming has been extensively used for years. The market value of greenhouse crops has reached $194 billion, occupying 49.8% of the total value of agricultural products while using only 10% of the cultivated land.[5] The global commercial greenhouse market value size is estimated to be at $68.7 billion by 2028.[6]

Humidity regulation of the greenhouses is the key for yield increase, and ecological footprint reduction. Because of condensation, high relative humidity (RH) can generate drips, which will promote the germination and spread of fungal pathogen spores such as *Botrytis* and powdery mildew,[7–10] leading to largescale outbreak of diseases and death of leaves or plants. Moreover, elevated humidity levels can disrupt plant transpiration, reducing crop yields and fostering issues such as algae growth due to standing water, accelerated insect proliferation, heightened safety hazards for workers, as well as condensation that can scatter light across ceilings and walls, affecting the photosynthesis process crucial for plant growth. Consequently, the maintenance of low RH in greenhouses is of utmost importance.

However, moisture is continuously generated by transpiration. It has always been challenging to regulate greenhouse humidity in an energy and cost-effective manner. The current solutions include both cultural practices such as precise watering,[11] adequate place spacing,[12] weed controlling,[13] as well as passive and active ventilation methods.[14–16] Passive ventilation replaces the high-humid inside air with the low-humid outside air by opening and closing the glazing

manually, facing problems of time consuming, labor intensive, and operator dependent.[17] Active ways for humidity control includes heat pump,[18,19] desiccants,[20–22] and heat exchangers.[22,23] Heat pumps have been reported effective as they condense the moisture in the air with evaporator coils. However, it costs nearly 64% of the initial capital of the greenhouse.[22] Solar-assisted liquid desiccants have been reported effective in dehumidification and temperature reduction for 5 to 7.5 °C.[24] Nevertheless, its applicability is constrained to regions with ample solar radiation. The incorporation of heating and venting systems to raise the dew point and replace highly humid air is energy-intensive,[25] demanding 0.7 kWh of energy per square meter, equivalent to 20% of a greenhouse's total energy expenditure.[26]

Implementing a more energy-efficient approach to humidity regulation can significantly reduce the energy consumption associated with agriculture, which currently amounts to as much as 1,872 trillion Btu per year in the United States.[27] In recent years, new technologies including functional greenhouse covers and Internet of Things have been developed to enable energy-independent, labor-independent, and high-yield greenhouses.[28–33] Major efforts have been devoted on the intelligent photovoltaic systems which regulate solar radiation, generate energy and control temperature.[34,35] However, advanced solutions for humidity regulation have not been explored in detail.

Another challenge is the global plastic pollution caused by the massive use of greenhouse glazing materials, including polyethylene, polycarbonate, and polyvinyl chloride.[36–38] With the growth of the greenhouse cover market to over $11.5 billion in 2021,[39] over 3 million tons of non-biodegradable agricultural plastic wastes are being produced each year.[40] Their degradation takes hundreds of years, which is a huge threat to the environment. Smart greenhouse glazing materials

and devices which can assist in climate control with desirable biodegradability are highly demanded.

In this paper, we present a new low-cost all-in-one solution based on humidity sensitive polyethylene glycol (PEG)/cellulose acetate (CA) blended films, which can be used as biodegradable smart glazing materials for greenhouses to adjust the humidity of the greenhouses through automatically opening the glazing for air circulation (the passive path), as well as humidity sensors to monitor the moisture level in the greenhouse and to control the ventilating system for accelerating the circulation (the active path).[41–44] Initially, we delved into techniques for producing consistent and transparent PEG/CA films. Subsequently, we conducted a quantitative assessment of the hygroscopic properties inherent to these films. Next, we gauged the effectiveness of PEG/CA films in humidity management within a laboratory-scale greenhouse, capitalizing on their capacity for humidity-activated shape change. Finally, we harnessed PEG/CA films in the construction of humidity sensors, enabling both humidity monitoring and controlling of the ventilating fan's speed to facilitate active air circulation and humidity reduction.

MATERIALS AND METHODS

Materials. Polyethylene glycol (PEG) (average M_n 20,000), cellulose acetate (average M_n 50,000), acetone absolute (>99.9%), and ethanol absolute (>99.9%) were all purchased from Sigma-Aldrich. Graphene particles were purchased from Techinstro, Inc. Medical polyurethane (PU) adhesive films (PERMEROLL Lite L34R15, 8 μm in thickness) were purchased from Nitto Denko, Inc. The Slygard 184 silicone elastomer kit was obtained from Dow Corning, Inc. Nafion films (N117-15) with thickness of 50 μm were purchased from FuelCellStore, US.

Manufacturing of the PEG/CA films. CA was dissolved in acetone at the weight ratio of 15 wt.%, and PEG was dissolved in the mix of ethanol and water (4:3 in volume) at weight ratio of 33 wt.%.

To manufacture the uniform single-layer PEG/CA blend film, the PEG and CA solutions were mixed at different PEG ratios ranging from 5 wt.% to 25 wt.%. As shown in Figure 1a, a film applicator was utilized for blade coating of the blended solution on silicon wafers at different thicknesses. The tested films thicknesses include 20 μm, 40 μm, 60 μm, 100 μm, and 150 μm. A suspended glass cover was applied on the blade coated film to reduce the evaporation rate and to protect the drying procedure at room temperature for 6 hours. A razor was used to cut around the edges of the film and to peel it off from the silicon substrate. In addition to the single-layer blended film, we also manufactured PEG+CA double layer film by blade coating PEG first and then the CA layer after the drying of the PEG layer (Figure 1b). Different thickness ratios between PEG and CA layers were tested, including 1:1, 1:2, 1:3, 1:4, 3:1, and 4:1.

Assessing the humidity-induced bending response of PEG/CA Films. As schematized in Figure 1c, a humidity controllable system was set up by connecting an acrylic chamber (132×40×40 cm^3) to a humidifier which released controllable amount of humid mist into the chamber from an opening at the upper surface of the chamber. There was a circular shape opening of 10 cm diameter at the opposite end. This way, the humidity coming out from the opening can be more uniform and controllable. The PEG/CA films were hung 2.5 cm away from the opening. The RH was monitored by a commercial humidity sensor (Sensirion SEK-SHT40-AD1B) attached close to the film. For the cycling test, the opening was firstly closed. After the humidity inside of the chamber became uniform, the cover on the opening was removed and the specimen was exposed to the humidity for 15 seconds. After which, the opening was closed for 30 seconds for the first cycle whereas the rest of cycles were closed for 45 seconds to ensure that the film was fully recovered to its original position. The cycle was repeated multiple times. Throughout this process, the films' responses were

documented through images and videos, which were subsequently analyzed using MATLAB to assess how the PEG/CA films reacted to fluctuations in humidity.

Quantifying bending angles via video analysis. For the analysis of experimental images and videos depicting the bending behavior of PEG/CA films, a custom video processing algorithm was developed using MATLAB. Initially, each video frame was cropped to isolate the region of interest, focusing solely on the film itself (see Figure 1d). Subsequently, a fiber-matrix filter was employed to accentuate the film's edges, enhancing their visibility. Additional processing techniques were then applied to smooth the film's edges and convert the image into a binary format, rendering the film region in white and the background in black (Figure 1e). To ensure accurate quantification, a boundary tracing function was applied specifically to the rightmost boundaries of each specimen to mitigate potential artifacts resulting from torsional effects during the bending process (Figure 1f). In order to determine the deflection of the specimens, the algorithm calculated the bending angle by computing the dot product between a reference vector (depicted as the yellow dotted line in Figure 1g) and tangent vectors associated with the specimen's edge. The reference vector was established by the algorithm based on the initial position of the specimen before bending. This process was executed for each frame within the videos, allowing for the capture of the bending angle of each boundary section.

Utilizing PEG/CA films for passive greenhouse humidity control. The humidity control chamber shown in Figure 1c was also utilized to simulate greenhouse conditions. To assess the PEG/CA film's ability to regulate the internal RH within the greenhouse, a circular PEG/CA film, 50 μm thick with a 10 cm diameter, was affixed externally, completely covering the opening. Sensirion humidity sensors were positioned at the center of the opening and 15 cm away from it on the chamber wall, both at the same height. By comparing data from these two humidity sensors,

we could contrast the humidity levels in areas with and without the smart cover. The humidifier was cycled on for 30 seconds and then off for 2 minutes, and this cycle was repeated at least 10 times.

Manufacturing of the PEG/CA humidity sensor. In this study, we employed the corona discharge enabled electrostatic printing (CEP) technology, as previously described, to print a binder-free graphene network onto the humidity-sensitive PEG/CA substrate, thereby producing the PEG/CA humidity sensors.[45] As illustrated in Figure 1h, the PEG/CA film was initially trimmed to a size of 5×1.27 cm^2. Subsequently, a 200 μm-thick layer of polydimethylsiloxane (PDMS) was applied to one side of the film. The uncoated surface was affixed to the underside of a polystyrene petri dish cap. Dry graphene powder was placed within the petri dish. The CEP system was employed to print the sample. After sealing the cap, a corona discharge (20 kV, 0.01 mA) was applied to the top of the petri dish. Driven by electrostatic forces, binder-free graphene adhered to the PEG/CA film within a mere 200 milliseconds. Subsequently, conductive threads were attached to serve as electrodes. Finally, a Nitto PU film was affixed to the printed side, functioning as a protective layer for the CEP-printed PEG/CA humidity sensor.

Active greenhouse humidity monitoring and regulation enabled by PEG/CA Humidity Sensor. The CEP-printed PEG/CA humidity sensor underwent testing by exposure to varying humidity levels. A multimeter (Agilent 34401A DMM) was employed to monitor resistance changes in the sensor throughout the humidity cycling process, mirroring the humidification cycles used in passive humidity regulation with PEG/CA films. The recorded data was then cross-referenced with humidity measurements obtained from the Sensirion sensor. For active humidity regulation, the PEG/CA humidity sensor was integrated with an Arduino Uno board and connected to a DC motor fan (12 V, 6000 RPM) designed to enhance greenhouse ventilation. A

microcontroller was programmed to monitor the resistance of the humidity sensor and compare it to a predefined threshold. When the sensor's resistance reached the designated threshold, the fan would be activated. Once the humidity dropped down to 60% RH, the humidifier was set to operate for 15 seconds to elevate the humidity level, thereby commencing the next cycle. Detailed flowchart of fabrication methodology can be found in Figure S5.

Evaluation of Volume Expansion Behavior in PEG/CA Films. Due to the small dimensions and rapid recovery of the films, traditional methods for measuring volume expansion were impractical. Instead, we determined the volume difference by measuring the change in the film's mass. We utilized the following Equation 1 to quantify the volume expansion,

$$V\% = \frac{\Delta V}{V_o} = \frac{V_f - V_o}{V_o} = \frac{(m_f - m_o)/\rho}{L \times W \times t} \quad (1)$$

where V represents volume, m represents mass, ρ signifies the density of water, and L, W, and t represent the length, width, and thickness of the film, respectively. Each film was initially weighed to obtain its initial weight m_o. Subsequently, it was fully immersed in a container filled with deionized water for 15 seconds. After the immersion process, the cleaned film was promptly transferred to the balance for measuring the weight m_f after absorbing water.

Finite element simulation of PEG/CA film's response to humidity. The bending behavior of the PEG/CA film was simulated using a hygroscopic swelling model in the COMSOL Multiphysics® software. In the simulation, the thin film was constrained in a similar manner to its physical counterpart in the experiments (i.e., fixed at one end and free at the rest of its boundaries as a cantilever beam). The hygroscopic swelling was governed by the Equation 2,

$$\varepsilon = \beta \times \Delta C \quad (2)$$

where ΔC is the mass concentration difference (i.e., water vapor in this study) and β is the coefficient of hygroscopic swelling of the material model. In this study, to better characterize the material property of the PEG/CA film, β values of the material were optimized in the finite element simulations to match the experimental bending angles measured from video processing.

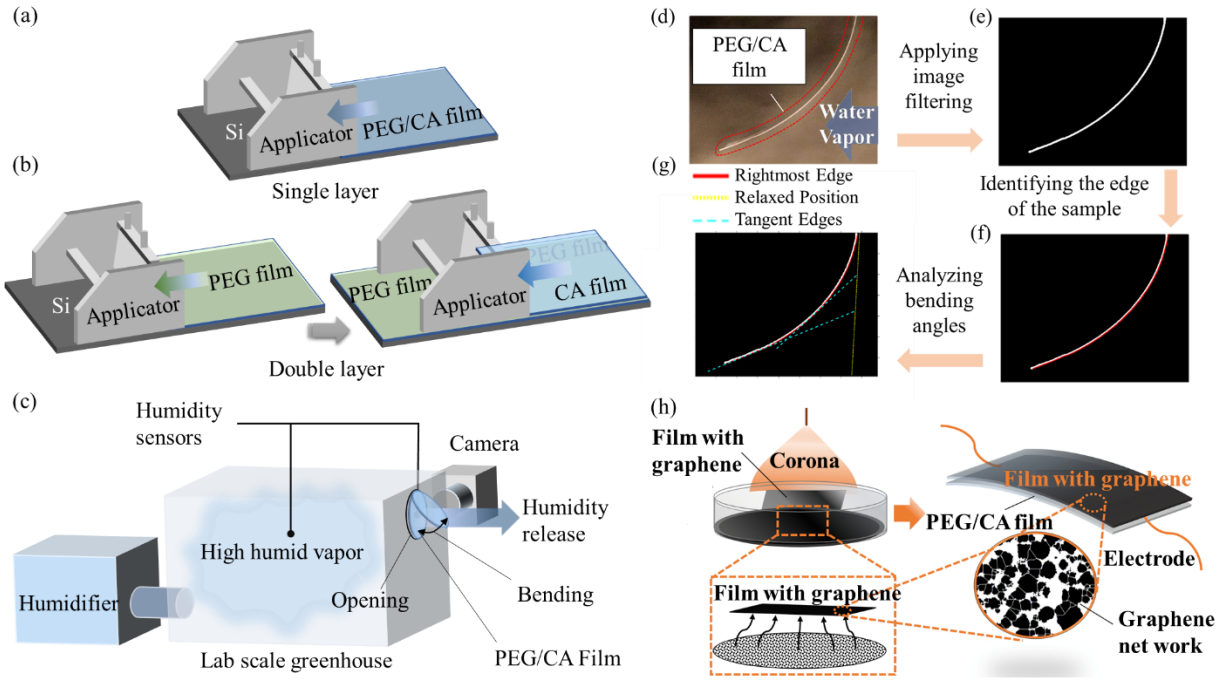

Figure 1. Experiment setups and procedures. (a) Blade coating of single-layer PEG/CA blend film; (b) Blade coating of double-layer film comprising PEG and CA layers; (c) Setup of the humidity chamber setup for evaluating bending behavior and assessing the PEG/CA films' capacity for regulating humidity in a lab-scale greenhouse; (d) Image capturing PEG/CA film bending under high humidity; (e) Processed image of the bending film; (f) Boundary tracing along the film; (g) Tangent vectors used for bending angle calculation; (h) Manufacturing process of CEP-printed PEG/CA humidity sensor.

RESULTS

Humidity activated bending of PEG/CA films. As demonstrated in Figure 2a (blue line), the water-absorbing component PEG plays a pivotal role in enhancing the hygroscopic swelling performance of the PEG/CA film. However, when the PEG concentration exceeded 20 wt.%, transparency and stiffness of the film were compromised. Hence, the recommended PEG blending ratio falls within the range of 10-20 wt.%. Throughout the subsequent experiments, all PEG/CA films contained 15 wt.% PEG.

The thickness of the PEG/CA film also has a significant impact on its bending behavior. As indicated by Figure 2a (pink line), 2b, and 2c, thinner films, such as those at 20 μm, could achieve a maximum bending angle of 66°. However, due to their reduced thickness, these films were more prone to twisting and exhibited less stable bending behavior. In contrast, 40 μm-thick films swiftly reached a bending angle of 70° within just 6 seconds and extended to 118° within 9 seconds. Remarkably, they efficiently reverted to their original straight state in a mere 10 seconds. In the case of 60 μm-thick PEG/CA films, they reached a maximum bending angle of 110° within 10 seconds and recovered after 25 seconds. Even the 100 μm film demonstrated an impressive maximum bending angle of 77°. However, when the film thickness increased to 150 μm, the maximum bending angle dropped to less than 30°. Thus, the recommended thickness range for PEG/CA films falls between 40 μm and 100 μm, ensuring both rapid, stable, and substantial bending behavior as well as effective recovery within a short time frame. Furthermore, as indicated in Figure S1 in the Supporting Information, the bending motion became more pronounced as the length-to-width ratio of the film increased.

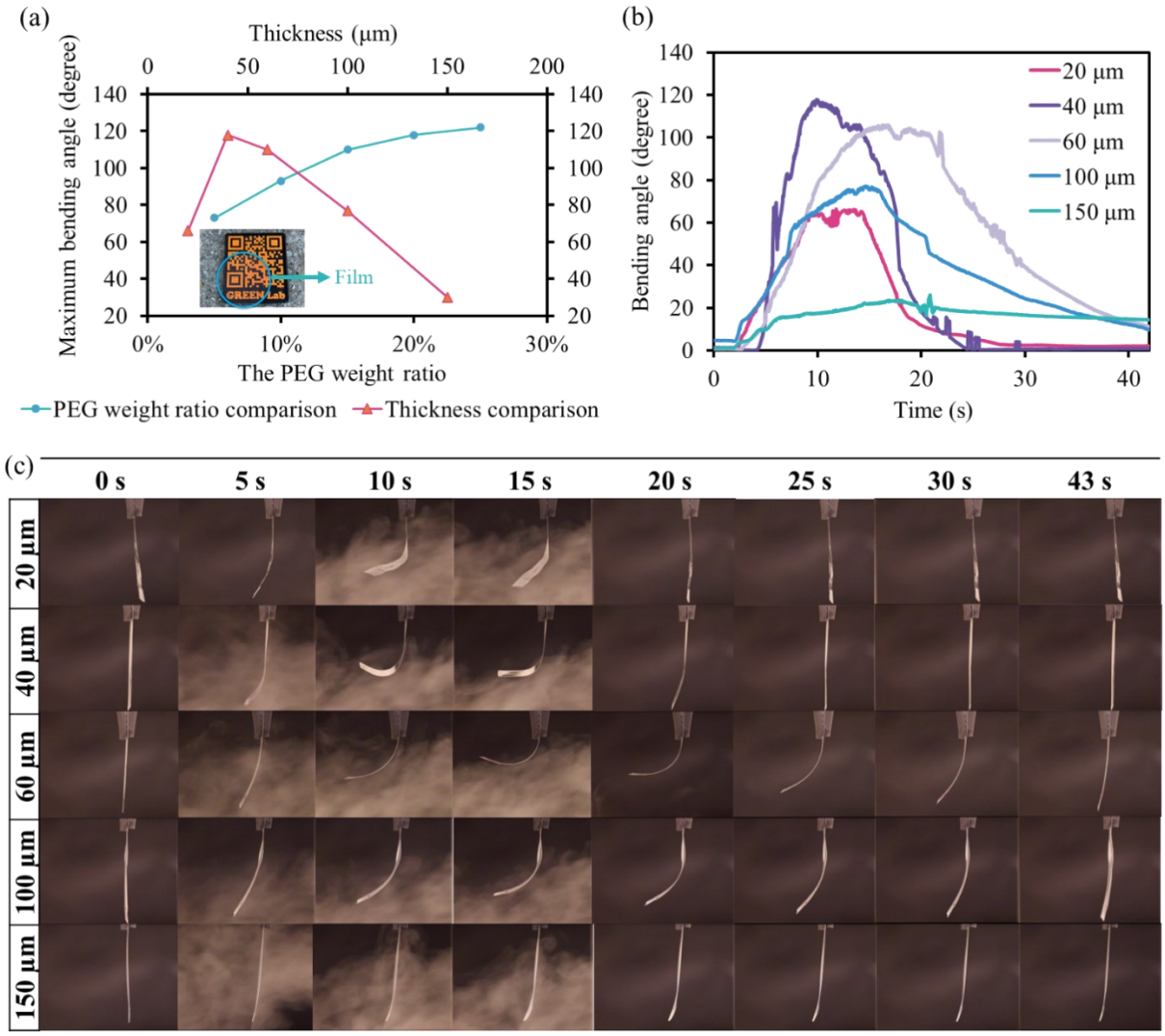

Figure 2. Humidity-induced bending response in single layer PEG/CA films under exposure to 90% relative humidity for 15 seconds at room temperature, followed by a 30-second recovery. (a) Maximum bending angle in response to varying PEG weight ratio (blue line) and film thicknesses (orange line); (b) Bending angle changes over time in single-layer PEG/CA films with different thicknesses (PEG ratio 15 wt.%); (c) Optical snapshots of PEG/CA films with different thicknesses.

Reversible bending response of PEG/CA films. The humidity activated bending behavior of PEG/CA films is reversible. In Figure 3, the 60 μm-thick PEG/CA film consistently achieved a

maximum bending angle of approximately 110° within 10 seconds in each cycle. Almost complete recovery was attained within 20 to 40 seconds, and this behavior was found to be repeatable across different cycles without any discernible degradation. Figure 3 also provides a comparative analysis of cycling behaviors in films with varying thicknesses. Among these, the 60 μm-thick film demonstrated the best repeatability and recovery performance. For the 20 μm-thick film, the behavior was similarly reversible, with a maximum bending angle of around 70° and a swift recovery to approximately 20° in less than 5 seconds. Likewise, the 150 μm-thick PEG/CA film displayed reversible behavior, albeit with a maximum bending angle of less than 30°. For effective humidity regulation in smart greenhouses, larger bending angles are preferable. Consequently, films with thicknesses ranging from 40 to 100 μm are recommended.

Moreover, as illustrated in Figure S2, our demonstration reveals that PEG/CA films exhibiting reversible responses to humidity present more promising prospects for humidity regulation in greenhouses compared to Nafion films which are non-degradable sulfonated tetrafluoroethylene-based fluoropolymer-copolymers. Additionally, Figure S3 illustrates that double-layer PEG+CA films also display commendable reversible responses to humidity, albeit with reduced reactivity when compared to their single-layer counterparts.

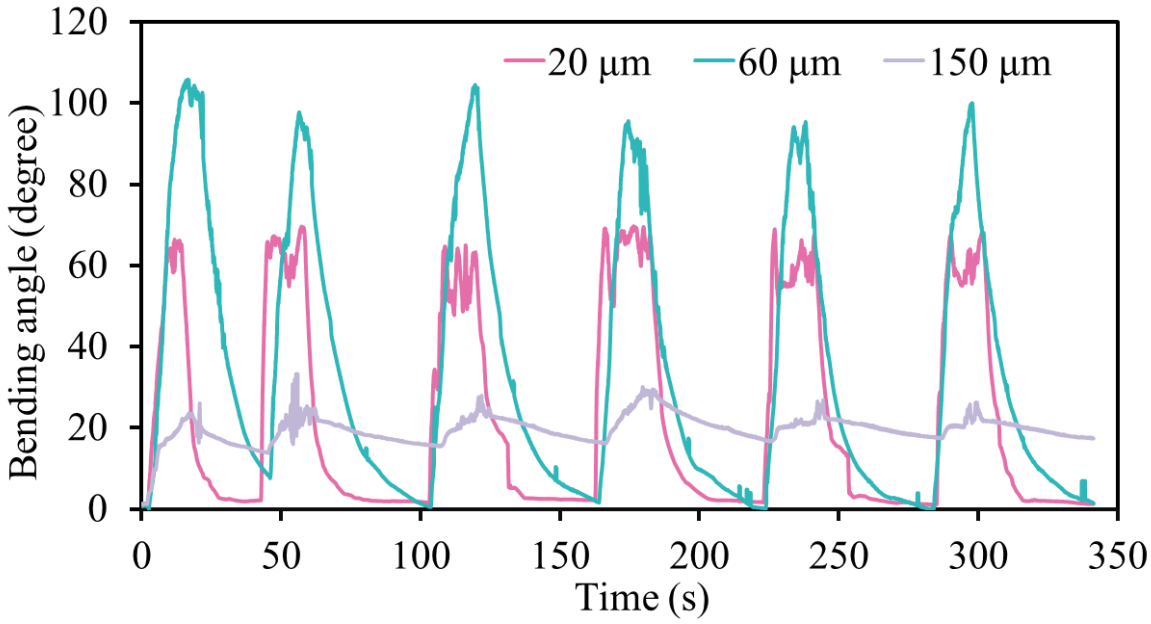

Figure 3. Assessment of cyclic humidity-induced bending angles in single-layer PEG/CA films, comparing the maximum bending angles for 20 µm, 60 µm, and 150 µm thicknesses

Humidity regulation of greenhouses with PEG/CA films as smart glazing. The effectiveness of PEG/CA films for regulating humidity in greenhouses was evaluated by applying the film to a lab scale greenhouse (Figure 1c). As illustrated in Figure 4a, when the humidifier was activated, the RH in the uncovered section of the greenhouse remained constant at approximately 95%, and it did not decrease even after the humidifier was turned off. In contrast, the area near the opening covered by the PEG/CA smart cover displayed high sensitivity to water vapor. When the humidity near this area surpassed 60%, the film promptly bent towards the side with lower humidity within seconds, thereby creating an open-air pathway for water vapor to escape from the greenhouse, as depicted in Figure 4b. The humidifier was initiated at the 0-second mark, and within moments, even before the visual detection of water vapor passing through the pathway, the smart cover began to bend, underscoring its exceptional sensitivity to water vapor. After 30 seconds, the humidifier was turned off for two minutes. Given the size of the acrylic greenhouse chamber, it took

approximately 60 seconds for the water vapor to be detected emerging from the pathway, prompting the cover to maintain its bent position. Around the 80-second mark, the greenhouse's humidity had decreased sufficiently, prompting the smart cover to gradually return to its original position. Ultimately, the humidity near the PEG/CA smart cover area decreased to as low as ~60% within 50 seconds, and the cover was almost fully closed at about the 150-second mark, just before commencing the second cycle.

As shown in Figure 4a, these humidification and dehumidification cycles were repeated at least 10 times. This humidity-activated opening and closing behaviour is highly reproducible, offering a straightforward, efficient, environmentally friendly, and continuous passive method for humidity regulation in greenhouses.

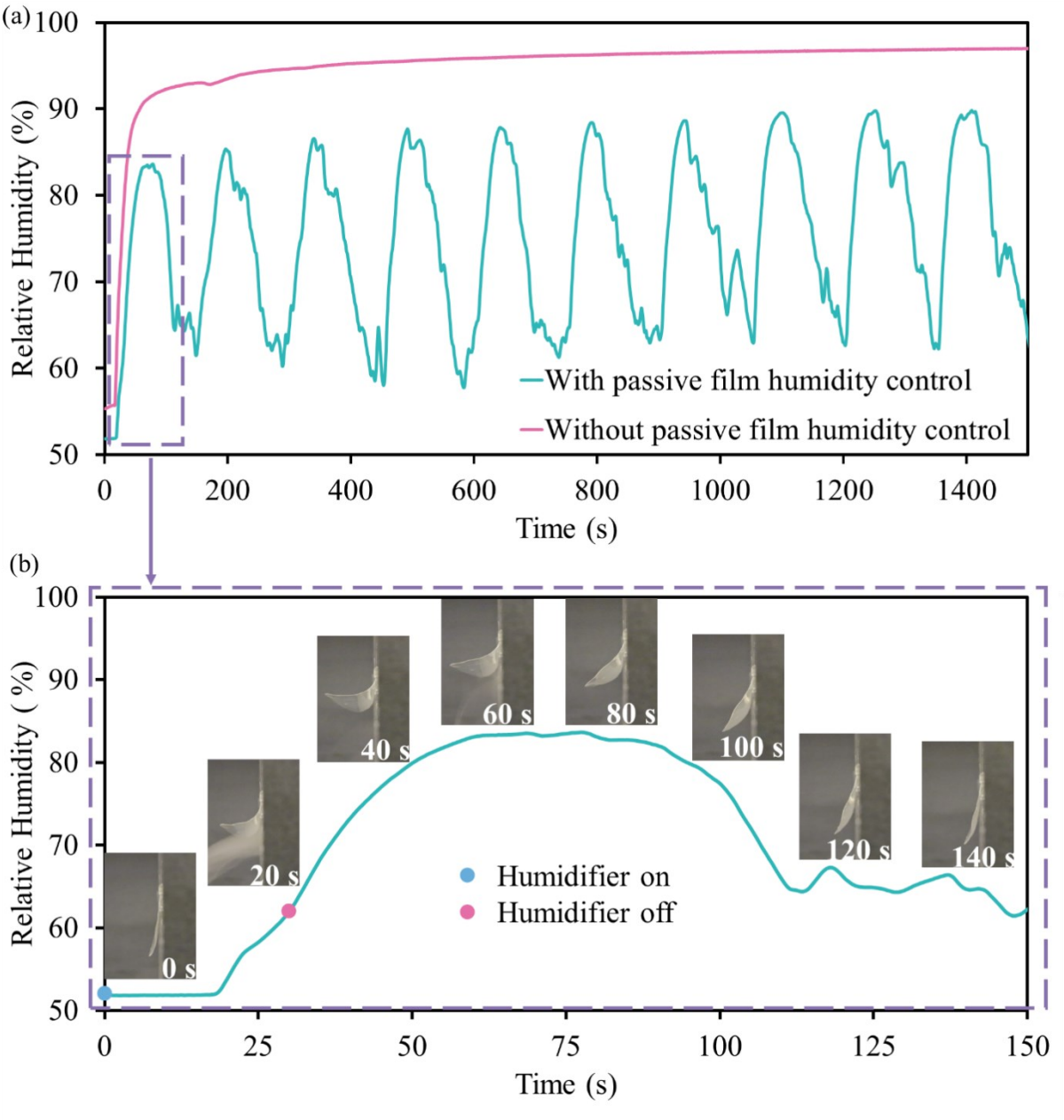

Figure 4. The humidity regulation efficacy of the PEG/CA smart film for greenhouse. (a) Comparison of relative humidity (RH) levels with and without the smart cover during humidity cycling; (b) Optical images of the opening and closing sequence of the smart cover throughout a single humidity test cycle, synchronized with the RH fluctuations induced by the PEG/CA film.

Monitoring humidity with CEP-printed PEG/CA humidity sensor. As depicted in Figure 1i, we applied the CEP printing process, as outlined in our prior publication, to print binder-free graphene powders onto the PEG/CA films [45]. Based on our prior work, it's important to note that the CEP-printed binder-free network is remarkably sensitive to the stress and strain exerted on it. The resistivity of the graphene network undergoes fluctuations with the bending and recovery of the PEG/CA substrate. This unique capability serves as the foundation for the creation of humidity sensors and their application in greenhouse humidity regulation.

In Figure 5a, we present the results of cyclic humidity monitoring, which involve a comparison between the data collected by the commercial Sensirion humidity sensor and our CEP-printed PEG/CA sensor. Zooming in on the cycles in Figure 5b, we observe that the resistivity of the PEG/CA sensor decreased as humidity levels rose. Notably, the PEG/CA sensor demonstrated an even faster response than the commercial sensor. When the humidifier was deactivated, the humidity reading decreased, leading to an increase in the sensor's resistivity. As the next cycle commenced, the resistivity of the PEG/CA sensor remained elevated until the commercially measured humidity surpassed 80%. This highlights the remarkable sensitivity of the CEP-printed sensor in the humidity range from 80% to 100%, which is particularly relevant for greenhouse operations. Greenhouses typically require humidity levels to be maintained below or around 80% during various stages of plant growth.[46] Subsequently, as the humidity reached approximately 80%, the resistivity decreased rapidly due to the bending behavior of the PEG/CA film. When the humidity returned to the ~80% mark, the resistivity increased once again. This entire process, as depicted in Figure 5a, illustrated excellent reversibility and cyclic performance. Therefore, the

CEP-printed PEG/CA sensor proves to be highly effective for humidity monitoring. Furthermore, in comparison to commercial humidity sensors, it exhibits greater sensitivity when humidity levels exceed ~80%, rendering it particularly well-suited for greenhouse humidity regulation. Additionally, its response time outpaces that of some of the top-performing humidity sensors currently available on the market.

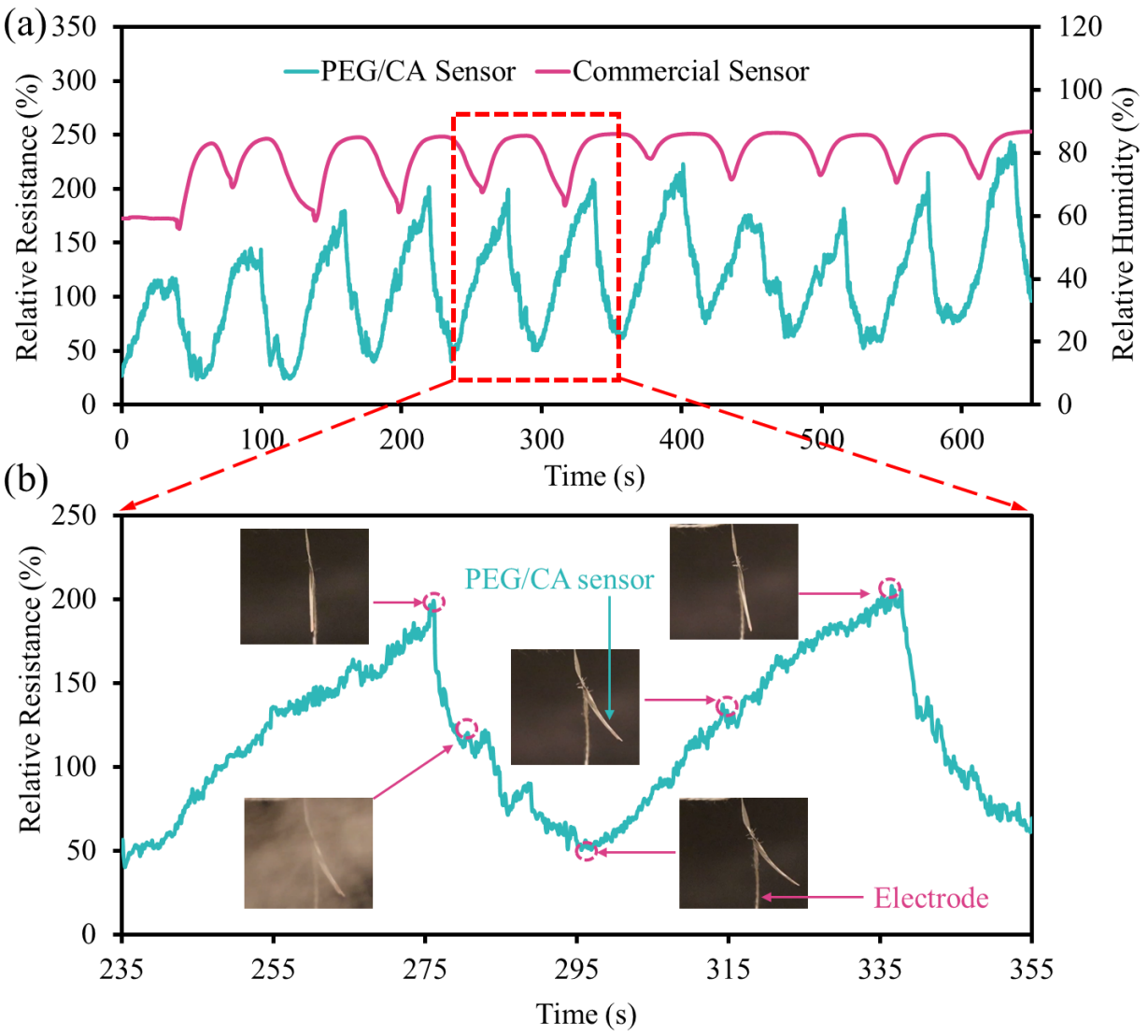

Figure 5. Variation in resistivity of the CEP-printed PEG/CA humidity sensor. (a) Comparative analysis of resistivity changes in the PEG/CA sensor with readings from a commercial humidity

sensor during cyclic humidity exposure; (b) In-depth examination of two cycles, illustrating the correlation between the bending of the PEG/CA sensor and changes in resistivity.

Active humidity regulation through control of ventilation fan using PEG/CA humidity sensor. The CEP printed PEG/CA sensor provides an effective way to transfer the humidity status to electric signal, which opens more possibilities for active humidity control. As demonstrated in Figure 6, the PEG/CA humidity sensor was utilized to control a ventilation fan. When the RH exceeded 80%, the relative resistance (resistance over the reference resistance when the film is flat) of the PEG/CA sensor dropped below a predetermined threshold value (approximately 150% relative resistance in this instance). This triggered the controller to activate the fan, which initiated the circulation of air and the expulsion of water vapor through the opening. Consequently, greenhouse humidity levels rapidly decreased to 60% or below. This experiment was successfully replicated, consistently yielding reproducible results, as depicted in Figure 6. Compared to the passive method, this active regulation method allows for faster and more efficient control of greenhouse humidity.

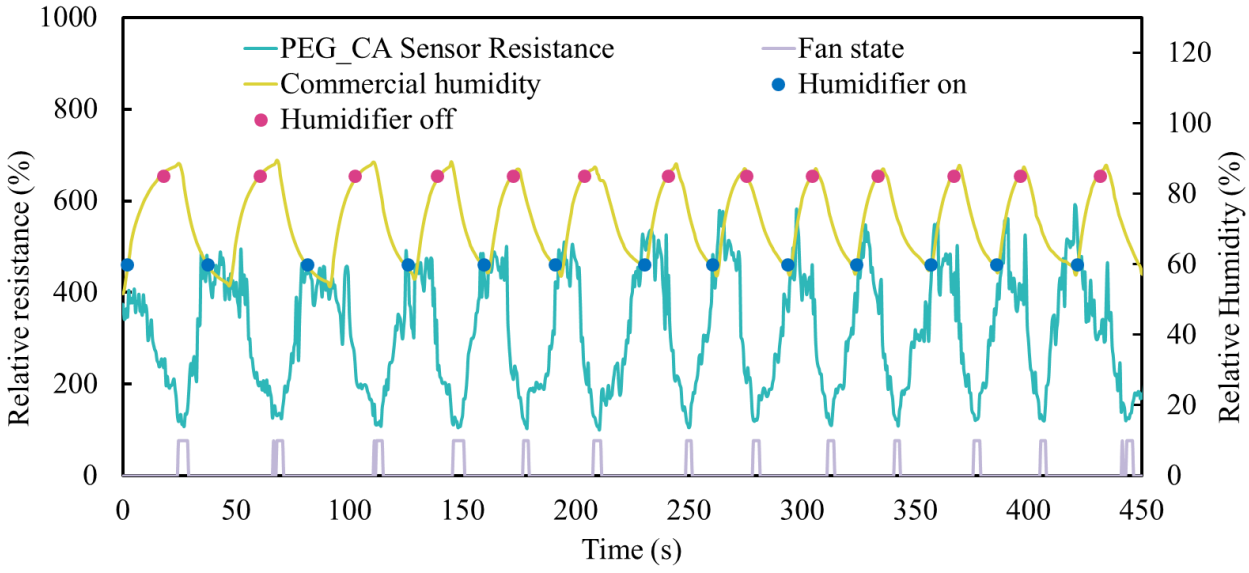

Figure 6. Humidity regulation impact of actively controlling the greenhouse ventilation fan with the CEP-printed PEG/CA humidity sensor.

DISCUSSION

Bending mechanism of the PEG/CA film. The bending response of the PEG/CA film to changes in humidity can be attributed to its remarkable hygroscopic expansion capability. As one side of the film is exposed to elevated humidity, it undergoes an increase in length due to the absorption of water molecules. This, in turn, induces internal strain within the film, resulting in its bending toward the lower humidity side. The hygroscopic expansion behavior of PEG/CA films was systematically assessed through both experimental and computational means. In Figure 7a, a comprehensive summary of the volume expansion in PEG/CA films with varying thicknesses is presented, following full immersion in water for 5 seconds, 15 seconds, and 30 seconds. It is readily apparent that longer immersion times lead to increased volume expansion. Notably, for films thinner than 60 μm, the volume expansion rate (indicated by the slope of the volume expansion line) from 5 seconds to 15 seconds exceeded that from 15 seconds to 30 seconds. This observation suggests that PEG/CA films possess the capacity to swell rapidly, with thinner films reaching full saturation more expeditiously. Conversely, for films thicker than 60 μm, the volume expansion rate remained relatively constant within the initial 30 seconds, affirming the swift responsiveness of PEG/CA films to elevated humidity levels. Furthermore, it's essential to highlight that thinner films exhibit more substantial volume expansion compared to their thicker counterparts. For instance, 20 μm-thick films achieved a volume expansion as high as 23.25% after 30 seconds, while 150 μm films only achieved an 8.37% expansion. This discrepancy provides a clear rationale for the observation of more substantial bending angles in thinner films ranging from 40 to 100 μm thickness that we recommended.

To gain deeper insights into the hygroscopic expansion characteristics of the PEG/CA material, we conducted COMSOL simulations to comprehensively analyze the bending behavior of PEG/CA films. Specifically, we computationally estimated the β for the PEG/CA polymer by comparing the maximum angular deflection (θ_{max}) in the simulation, which incorporated varying β values, with the experimental value. This iterative process aimed to minimize the disparity in angular deflection. Our estimation relied on psychrometric data related to water vapor and the laboratory environment, in conjunction with the maximum deflection angle observed at the midpoint of each film specimen with distinct thicknesses. As depicted in Figure 7b, we calculated the β value to be 0.142 ± 0.025 m^3/kg, with a 95% confidence interval. This calibrated β for the PEG/CA material equips us to predict the bending behavior of PEG/CA films with arbitrary thickness under specific humidity conditions. Such predictive capabilities can significantly facilitate the design of humidity sensors based on PEG/CA.

For instance, Figure 7c provides an illustration of the simulated angular deflection (left), the distribution of the first principal strain (middle), and the Von Mises stress (right) when a 60 μm-thick PEG/CA specimen was exposed to an 80% RH. Impressively, the simulated deflection shape closely aligns with the experimental observations, as seen in Figure 1d, underscoring the validity and accuracy of our simulations.

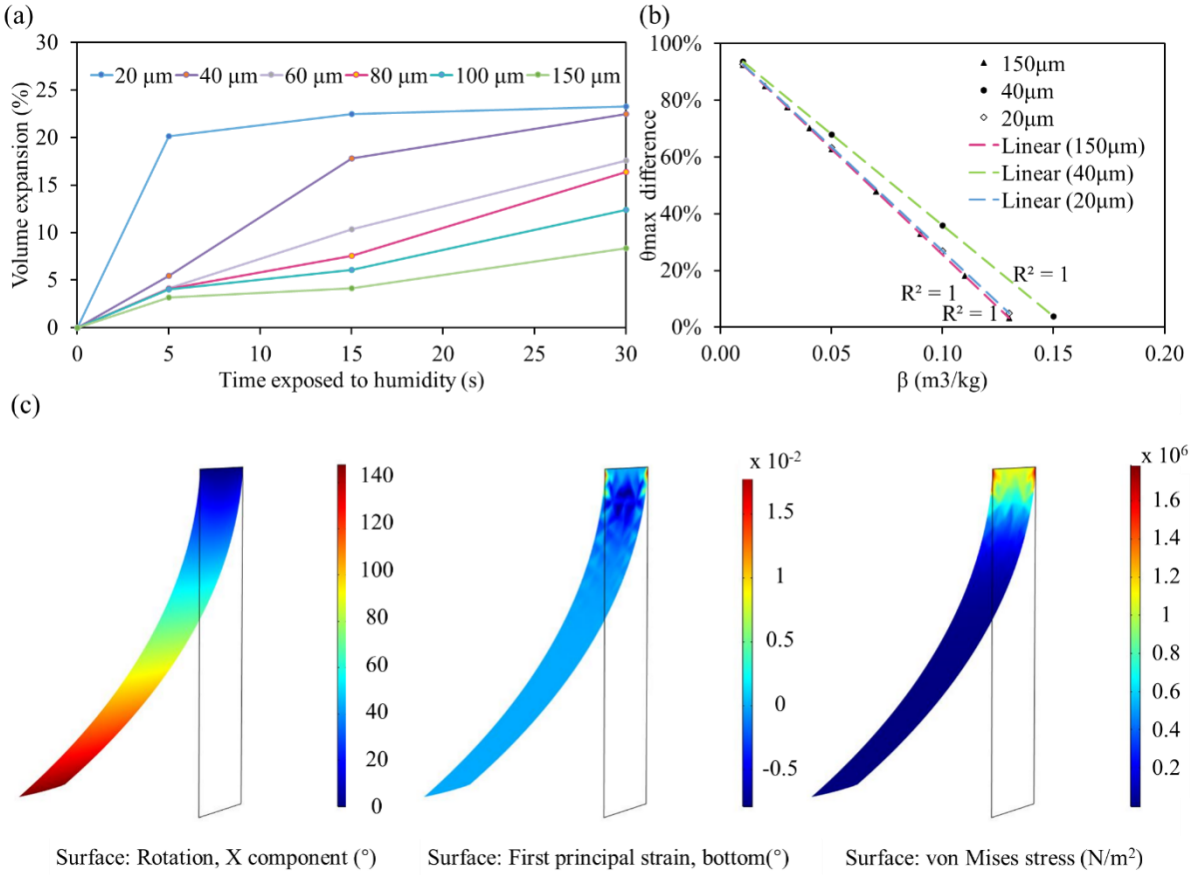

Figure 7. The bending of the PEG/CA films caused by their hygroscopic expansion property. (a) Volume expansion of PEG/CA films with varying thicknesses during full immersion in water for 5 seconds, 15 seconds, and 30 seconds; (b) Calibration of the coefficient of hygroscopic swelling (β) for PEG/CA material; (c) Simulated distribution illustrating angular deflection (left), first principal strain (middle), and von mises stress (right) in a 60 μm-thick PEG/CA film exposed to 80% relative humidity.

Sensing mechanism of the CEP-fabricated PEG/CA humidity sensor. The alterations in resistance observed in the CEP-printed PEG/CA humidity sensor were postulated to stem from the microstructural modifications within the binder-free graphene network. These changes occur as a response to variations in the shape of the PEG/CA substrate induced by hygroscopic swelling and

bending.[45,47] To scrutinize the electrical properties of the graphene networks fabricated through the CEP method, a meticulous finite element analysis was executed by employingthe microstructures of the graphene network. In particular, an open-source MATLAB algorithm, namely DigiSim, was initially embraced and subsequently tailored to construct computational material models derived from microscopic images of the graphene networks.[48] The algorithm commenced by employing image filtering techniques to convert optical images of the samples, encompassing both the graphene particles and the voids between them, into binary images. These binary images were then subjected to a vectorization function to extract their geometric characteristics, generating a corresponding DXF design file. This file served as the material model for finite element simulations performed using the AC/DC Module within the COMSOL Multiphysics software.

In order to investigate the influence of humidity-induced bending behaviour on the electrical properties of the CEP-fabricated graphene networks (i.e., the sensing mechanism), optical microscopy was employed to capture the microstructures of the samples at varying bending angles (i.e., 0º, 60º, and 108º), as depicted in Figure 8a-8c. Subsequently, these images (Figure 8a-8c corresponding to 0º, 60º, and 108º bending angles) were converted into computational material models using the MATLAB algorithm described earlier. For each material model, ground and terminal boundaries were assigned to the left and right edges, respectively. Furthermore, a constant current of 2 mA was introduced into the material network, mirroring the procedure used in the DMM's resistance measurement mode. Figure 8d-8f illustrate the simulated electrical potential distributions within the graphene networks when the substrate was bent to 0º, 60º, and 108º, respectively. It is evident that the electrical potential became more uniformly distributed as the substrate's bending angle increased, signifying that the graphene particles became denser due to the compression induced by deflection.

It is worth noting that the microscopic setup employed to capture these images featured 3D-printed PDMS as imagingsupports. These PDMS supports precisely replicated the deflection shapes observed in the 60-µm thick PEG/CA films, with the graphene networks positioned on the compression side, as illustrated in Figure S4. Consequently, the computational study corroborated the hypothesis that the sensing functionality of the CEP-fabricated humidity sensors stemmed from the configuration change in the graphene networks during bending. Specifically, the graphene particles became more densely packed, creating additional electrically conductive pathways during bending, resulting in a decrease in measured resistance.

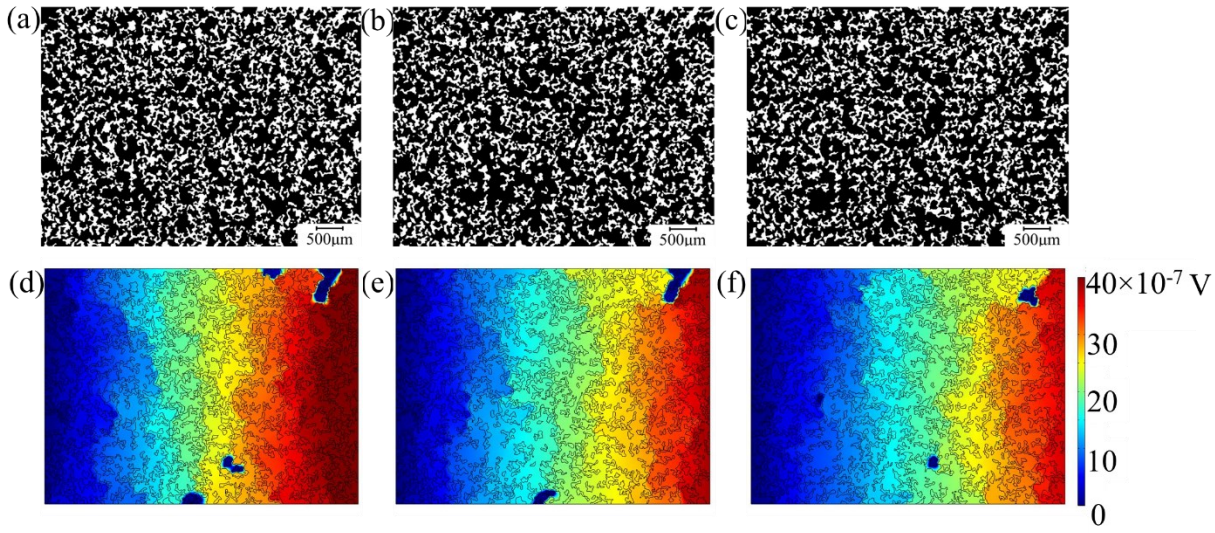

Figure 8. Investigating the influence of bending on electrical properties of CEP-fabricated graphene networks. (a-c) Optical micrographs of graphene networks with substrate bending angles of 0, 60, and 108 degrees, respectively. Graphene networks are depicted in black, while voids are shown in white. (d-f) Simulated electrical potential distributions in the material network for the scenarios depicted in (a-c), respectively.

Energy saving analysis. Drawing from the findings above, we claim that employing both passive and active methods for greenhouse humidity regulation can intelligently conserve energy. Typically, greenhouse ventilation systems consume roughly 5.38 to 10.76 kilowatt-hours per square meters per year.[49,50] However, with a refined sensing and variable speed control system, the energy consumption of these fans can be reduced by around 25%.[51] According 2019 U.S. Census of Horticulture Specialties, the greenhouse operations in the USA cover a total area of 5.26×10^6 square meters.[52] Thus, implementing our smart active fan control system could potentially yield annual energy savings ranging from about 7.07 to 14.15 gigawatt-hours in the US. Conversely, considering that the operating time of the vent motor in a natural ventilation system typically amounts to approximately 0.5 hours per day, compared to an average of 5 hours per day for the fan-controlled active system, adopting a passive system that facilitates natural ventilation without controlled fans could lead to a substantial 75% reduction in energy consumption.[49,53] This translates to annual energy savings ranging from approximately 21.22 to 42.45 gigawatt-hours in the US. Therefore, in total, the full introduction of the passive + active PEG/CA humidity regulation system can save up to 56.6 gigawatt-hours energy for the US.

Potential application in area where outdoor humidity is higher than indoor. As mentioned earlier, the optimal humidity level for greenhouse crop production typically ranges below or around 80%.[46] In regions where humidity levels exceed 80%, employing a sensor-controlled dehumidifier would be more effective than utilizing a fan for humidity reduction in conjunction with our active method. Moreover, with the passive method, we can incorporate a polyethylene terephthalate (PET) film on the exterior of our smart glazing cover to prevent excessive outdoor humidity from triggering the bending of the cover and infiltrating the greenhouse.

CONCLUSIONS

To conclude, we have successfully demonstrated the fabrication of biodegradable smart glazing materials for greenhouse humidity regulation using PEG/CA blend films. Our findings indicate that films with a thickness ranging from 40 μm to 100 μm exhibit rapid, stable, and sufficient bending behavior, along with faster recovery. The coefficient of hygroscopic swelling of the PEG/CA material system was calibrated, which can facilitate the prediction of the bending behavior of the PEG/CA films of an arbitrary thickness under a certain humidity. Leveraging the bending behavior of PEG/CA films, we have successfully demonstrated effective and repeatable greenhouse humidity regulation to as low as 60% RH through the use of PEG/CA covers. Combined with the CEP technology, we have fabricated PEG/CA humidity sensors that enable active air circulation and humidity reduction by controlling a built-in ventilating fan within a lab-scale greenhouse. These sensors have demonstrated stability, repeatability, and excellent sensitivity performance compared with one of the best commercial humidity sensors. We have also investigated the sensing mechanism of the CEP-fabricated PEG/CA humidity sensors via microscopic imaging coupled with finite element simulations. It was found that the CEP-fabricated graphene networks became more compacted upon bending motions, which could render the material networks more conductive and generate measurable decrease in the resistance of sensors. In summary, our results provide robust evidence supporting the application of biodegradable PEG/CA films as smart glazing materials for effective greenhouse humidity regulation through both passive and active ways. These findings underscore the enormous potential for scaling up to commercial greenhouse operations, presenting a promising avenue for addressing global food shortages and famine while prioritizing sustainability.

ASSOCIATED CONTENT

Supporting Information

The following files are available free of charge.

Supporting Information 1: The bending motion of single layer 60 μm-thick PEG/CA films with different lengths; Comparing the cyclic humidity induced bending behavior of 60 μm PEG/CA film and 50 μm Nafion film; The humidity induced bending behavior of double layer PEG+CA films; Setup for microscopic imaging of graphene PEG/CA film under bending (PDF).

Supporting Information 2: Video 1 shows the bending behavior of the 60 μm PEG/CA film under 15 seconds humidifying process (MP4).

AUTHOR INFORMATION

Corresponding Authors

Ying Zhong − *Sauvage Laboratory for Smart Materials, School of Materials Science and Engineering, Harbin Institute of Technology (Shenzhen), The University City in Shenzhen, Shenzhen, Guangdong 518055, China*; Email: zhongy@hit.edu.cn

Long Wang – *Department of Civil and Environmental Engineering, California Polytechnic State University, 1 Grand Ave, San Luis Obispo, CA 93407, USA*; E-mail: lwang38@calpoly.edu

Wenbin Mao − *Department of Mechanical Engineering, University of South Florida, 4202 E. Fowler Ave, Tampa, FL 33620, USA*; Email: wmao@usf.edu

Authors

Zijian Weng − Department of Mechanical Engineering, University of South Florida, 4202 E. Fowler Ave, Tampa, FL 33620, USA; Email: zweng@usf.edu

Omar Khater − Department of Mechanical Engineering, University of South Florida, 4202 E. Fowler Ave, Tampa, FL 33620, USA; Email: okhater@usf.edu

Vladislav Paley − Department of Mechanical Engineering, University of South Florida, 4202 E. Fowler Ave, Tampa, FL 33620, USA; Email: paleyv@usf.edu

Nathan K. Kessenich − Department of Mechanical Engineering, California Polytechnic State University, San Luis Obispo, CA 93407, USA; E-mail: nkesseni@calpoly.edu

Logan G. Schmid − Department of Biomedical Engineering, California Polytechnic State University, San Luis Obispo, CA 93407, USA; E-mail: lgschmid@calpoly.edu

Marco U. Lam − Department of Mechanical Engineering, University of South Florida, 4202 E. Fowler Ave, Tampa, FL 33620, USA; Email: marco4@usf.edu

Abhishek Dyade − Department of Mechanical Engineering, University of South Florida, 4202 E. Fowler Ave, Tampa, FL 33620, USA; Email: abhishekdyade@usf.edu

Zengyu Zhan − Department of Mechanical Engineering, University of South Florida, 4202 E. Fowler Ave, Tampa, FL 33620, USA; Email: zengyuzhan@usf.edu

Author Contrubutions

Zijian Weng: Validation, Methodology, Formal analysis, Investigation, Data Curation, Writing – Original Draft, Visualization, **Omar Khater**: Validation, Formal analysis, Investigation, Methodology, Data Curation, Writing – Original Draft, **Vladislav Paley**: Methodology,

Investigation, **Nathan K. Kessenich**: Software, Data curation, **Logan G. Schmid**: Software, **Marco U. Lam**: Validation, Investigation, **Abhishek Dyade**: Validation, Investigation, **Zengyu Zhan**: Investigation, **Wenbin Mao**: Conceptualization, Writing - Review & Editing, Supervision, Project administration, Funding acquisition, **Long Wang**: Conceptualization, Writing - Review & Editing, Supervision, Project administration, Funding acquisition, **Ying Zhong**: Conceptualization, Resources, Writing - Original Draft, Supervision, Project administration, Funding acquisition

Notes

The authors declare that they have no known competing financial interests or personal relationships that could have appeared to influence the work reported in this paper.

Acknowledgements

Y. Zhong acknowledges the support from the National Natural Science Foundation of China under grant number 52375321. W. Mao acknowledges the support from the U.S. National Science Foundation under grant number 2114216. L. Wang acknowledges the support from the U.S. National Science Foundation under grant number 2114223.

References

(1) World Food Programme. https://www.wfp.org/stories/45-million-people-are-famines-door (accessed 2024-03-05).

(2) Alaanuloluwa Ikhuoso, O.; Adegbeye, M. J.; Elghandour, M. M. Y.; Mellado, M.; Al-Dobaib, S. N.; Salem, A. Z. M. Climate Change and Agriculture: The Competition for Limited Resources amidst Crop Farmers-Livestock Herding Conflict in Nigeria - A Review. *J. Clean. Prod.* **2020**, *272*, 123104. https://doi.org/10.1016/J.JCLEPRO.2020.123104.

(3) Kakaei, H.; Nourmoradi, H.; Bakhtiyari, S.; Jalilian, M.; Mirzaei, A. Effect of COVID-19 on Food Security, Hunger, and Food Crisis. In *COVID-19 and the Sustainable Development Goals*; Elsevier, 2022; pp 3–29. https://doi.org/10.1016/B978-0-323-91307-2.00005-5.

(4) Nchasi, G.; Mwasha, C.; Shaban, M. M.; Rwegasira, R.; Mallilah, B.; Chesco, J.; Volkova, A.; Mahmoud, A. Ukraine's Triple Emergency: Food Crisis amid Conflicts and COVID-19 Pandemic. *Heal. Sci. Reports* **2022**, *5* (6), e862. https://doi.org/10.1002/HSR2.862.

(5) USDA National Agricultural Statistics Service. https://www.nass.usda.gov/AgCensus/ (accessed 2024-03-05).

(6) MarketsandMarkets. https://www.marketsandmarkets.com/Market-Reports/commercial-greenhouse-market-221045451.html (accessed 2024-03-05).

(7) Asalf, B.; Onofre, R. B.; Gadoury, D. M.; Peres, N. A.; Stensvand, A. Pulsed Water Mists for Suppression of Strawberry Powdery Mildew. *Plant Dis.* **2021**, *105* (1), 71–77. https://doi.org/10.1094/PDIS-04-20-0735-RE.

(8) Fedele, G.; Brischetto, C.; Rossi, V. Biocontrol of Botrytis Cinerea on Grape Berries as Influenced by Temperature and Humidity. *Front. Plant Sci.* **2020**, *11*. https://doi.org/10.3389/fpls.2020.01232.

(9) Li, T.; Zhou, J.; Li, J. Combined Effects of Temperature and Humidity on the Interaction between Tomato and Botrytis Cinerea Revealed by Integration of Histological Characteristics and Transcriptome Sequencing. *Hortic. Res.* **2023**, *10* (2), uhac257. https://doi.org/10.1093/HR/UHAC257.

(10) Sun, S.; Lian, S.; Feng, S.; Dong, X.; Wang, C.; Li, B.; Liang, W. Effects of Temperature and Moisture on Sporulation and Infection by Pseudoperonospora Cubensis. *Plant Dis.* **2017**, *101* (4), 562–567. https://doi.org/10.1094/PDIS-09-16-1232-RE.

(11) Abdul-Rudha Husaein, F.; Ahmad, M.; Kadhim Rashid, A. Development of Automated Powered Precise Watering System for Large Framing in Desert. *Int. J. Sci. Eng. Investig.* **2018**, *7* (75), 1.

(12) Fox, J. A.; Adriaanse, P.; Stacey, N. T. Greenhouse Energy Management: The Thermal Interaction of Greenhouses with the Ground. *J. Clean. Prod.* **2019**, *235*, 288–296. https://doi.org/10.1016/J.JCLEPRO.2019.06.344.

(13) NC State Extension Publications. https://content.ces.ncsu.edu/greenhouse-weed-control

(accessed 2024-03-05).

(14) Abedrabboh, O.; Koç, M.; Biçer, Y. Comparative Thermoeconomic Assessment of Renewable-Driven Hybrid-Cooled Sustainable Greenhouses for Subtropical Regions. *Energy Convers. Manag.* **2024**, *300*, 117990. https://doi.org/10.1016/J.ENCONMAN.2023.117990.

(15) Coomans, M.; Allaerts, K.; Wittemans, L.; Pinxteren, D. Monitoring and Energetic Performance of Two Similar Semi-Closed Greenhouse Ventilation Systems. *Energy Convers. Manag.* **2013**, *76*, 128–136. https://doi.org/10.1016/J.ENCONMAN.2013.07.028.

(16) RT. https://rtmagazine.com/disorders-diseases/critical-care/icu-ventilation/time-to-rethink-active-versus-passive-humidification/ (accessed 2024-03-05).

(17) Amani, M.; Foroushani, S.; Sultan, M.; Bahrami, M. Comprehensive Review on Dehumidification Strategies for Agricultural Greenhouse Applications. *Appl. Therm. Eng.* **2020**, *181*, 115979. https://doi.org/10.1016/J.APPLTHERMALENG.2020.115979.

(18) Aye, L.; Fuller, R. J.; Canal, A. Evaluation of a Heat Pump System for Greenhouse Heating. *Int. J. Therm. Sci.* **2010**, *49* (1), 202–208. https://doi.org/10.1016/J.IJTHERMALSCI.2009.07.002.

(19) Hassanien, R. H. E.; Li, M.; Tang, Y. The Evacuated Tube Solar Collector Assisted Heat Pump for Heating Greenhouses. *Energy Build.* **2018**, *169*, 305–318. https://doi.org/10.1016/J.ENBUILD.2018.03.072.

(20) Chen, X.; Liang, H.; Wu, G.; Feng, C.; Tao, T.; Ji, Y.; Ma, Q.; Tong, Y. Coupled Heat and Humidity Control System of Narrow-Trough Solar Collector and Solid Desiccant in Chinese Solar Greenhouse: Analysis of Optical / Thermal Characteristics and Experimental Study. *Energy* **2023**, *273*, 127198. https://doi.org/10.1016/J.ENERGY.2023.127198.

(21) Jaradat, M.; Albatayneh, A.; Alsotary, O.; Hammad, R.; Juaidi, A.; Manzano-Agugliaro, F. Water Harvesting System in Greenhouses with Liquid Desiccant Technology. *J. Clean. Prod.* **2023**, *414*, 137587. https://doi.org/10.1016/J.JCLEPRO.2023.137587.

(22) Pasqualin, P.; Lefers, R.; Mahmoud, S.; Davies, P. A. Comparative Review of Membrane-Based Desalination Technologies for Energy-Efficient Regeneration in Liquid Desiccant Air Conditioning of Greenhouses. *Renew. Sustain. Energy Rev.* **2022**, *154*, 111815. https://doi.org/10.1016/J.RSER.2021.111815.

(23) Barbaresi, A.; Maioli, V.; Bovo, M.; Tinti, F.; Torreggiani, D.; Tassinari, P. Application of Basket Geothermal Heat Exchangers for Sustainable Greenhouse Cultivation. *Renew. Sustain. Energy Rev.* **2020**, *129*, 109928. https://doi.org/10.1016/J.RSER.2020.109928.

(24) Buker, M. S.; Riffat, S. B. Recent Developments in Solar Assisted Liquid Desiccant Evaporative Cooling Technology—A Review. *Energy Build.* **2015**, *96*, 95–108. https://doi.org/10.1016/J.ENBUILD.2015.03.020.

(25) Bronchart, F.; De Paepe, M.; Dewulf, J.; Schrevens, E.; Demeyer, P. Thermodynamics of Greenhouse Systems for the Northern Latitudes: Analysis, Evaluation and Prospects for

Primary Energy Saving. *J. Environ. Manage.* **2013**, *119*, 121–133. https://doi.org/10.1016/J.JENVMAN.2013.01.013.

(26) Liu, S.; Lee, S.; Jeong, C.-H.; Yeo, M.-S. Field Study of Heat Pump-Assisted Hybrid Desiccant Cooling System for Thermal Environment Control and Energy Consumption under Different Load Patterns. *Case Stud. Therm. Eng.* **2022**, *36*, 102170. https://doi.org/10.1016/J.CSITE.2022.102170.

(27) United States Department of Agriculture Trends in U.S. https://www.ers.usda.gov/publications/pub-details/?pubid=74661 (accessed 2024-03-05).

(28) Baeza, E. J.; van Breugel, A. J. B.; Hemming, S.; Stanghellini, C. Smart Greenhouse Covers: A Look into the Future. *Acta Hortic.* **2020**, *1268*, 213–224. https://doi.org/10.17660/ACTAHORTIC.2020.1268.28.

(29) Castañeda-Miranda, A.; Castaño-Meneses, V. M. Internet of Things for Smart Farming and Frost Intelligent Control in Greenhouses. *Comput. Electron. Agric.* **2020**, *176*, 105614. https://doi.org/10.1016/J.COMPAG.2020.105614.

(30) Petropoulou, A. S.; van Marrewijk, B.; de Zwart, F.; Elings, A.; Bijlaard, M.; van Daalen, T.; Jansen, G.; Hemming, S. Lettuce Production in Intelligent Greenhouses—3D Imaging and Computer Vision for Plant Spacing Decisions. *Sensors* **2023**, *23* (6), 2929. https://doi.org/10.3390/S23062929.

(31) Sappat, A.; Wisitsoraat, A.; Sriprachuabwong, C.; Jaruwongrungsee, K.; Lomas, T.; Tuantranont, A. Humidity Sensor Based on Piezoresistive Microcantilever with Inkjet Printed PEDOT/PSS Sensing Layers. *ECTI-CON 2011 - 8th Electr. Eng. Electron. Comput. Telecommun. Inf. Technol. Assoc. Thail. - Conf.* **2011**, 34–37. https://doi.org/10.1109/ECTICON.2011.5947764.

(32) Turkani, V. S.; Maddipatla, D.; Narakathu, B. B.; Saeed, T. S.; Obare, S. O.; Bazuin, B. J.; Atashbar, M. Z. A Highly Sensitive Printed Humidity Sensor Based on a Functionalized MWCNT/HEC Composite for Flexible Electronics Application. *Nanoscale Adv.* **2019**, *1* (6), 2311–2322. https://doi.org/10.1039/c9na00179d.

(33) Wang, Q.; Tong, J.; Wang, N.; Chen, S.; Sheng, B. Humidity Sensor of Tunnel-Cracked Nickel@polyurethane Sponge for Respiratory and Perspiration Sensing. *Sensors Actuators, B Chem.* **2021**, *330*, 129322. https://doi.org/10.1016/j.snb.2020.129322.

(34) Pérez-Alonso, J.; Pérez-García, M.; Pasamontes-Romera, M.; Callejón-Ferre, A. J. Performance Analysis and Neural Modelling of a Greenhouse Integrated Photovoltaic System. *Renew. Sustain. Energy Rev.* **2012**, *16* (7), 4675–4685. https://doi.org/10.1016/J.RSER.2012.04.002.

(35) Yang, Z.; Zhang, Y.; Xiao, H.; Zhuang, R.; Liang, X.; Cui, M.; Li, X.; Zhao, J.; Yuan, Q.; Yang, R.; Wang, B.; Shi, W. Comprehensive Test of Ultra-Efficient Air Conditioner with Smart Evaporative Cooling Ventilation and Photovoltaic. *Energy Convers. Manag.* **2022**, *254*, 115267. https://doi.org/10.1016/J.ENCONMAN.2022.115267.

(36) Cascone, S.; Ingrao, C.; Valenti, F.; Porto, S. M. C. Energy and Environmental Assessment

of Plastic Granule Production from Recycled Greenhouse Covering Films in a Circular Economy Perspective. *J. Environ. Manage.* **2020**, *254*, 109796. https://doi.org/10.1016/J.JENVMAN.2019.109796.

(37) Maraveas, C. Environmental Sustainability of Greenhouse Covering Materials. *Sustainability* **2019**, *11* (21), 6129. https://doi.org/10.3390/SU11216129.

(38) Parlato, M. C. M.; Valenti, F.; Porto, S. M. C. Covering Plastic Films in Greenhouses System: A GIS-Based Model to Improve Post Use Suistainable Management. *J. Environ. Manage.* **2020**, *263*, 110389. https://doi.org/10.1016/J.JENVMAN.2020.110389.

(39) MarketsandMarkets. https://www.marketsandmarkets.com/Market-Reports/greenhouse-film-market-179191625.html (accessed 2024-03-05).

(40) Andreeßen, C.; Steinbüchel, A. Recent Developments in Non-Biodegradable Biopolymers: Precursors, Production Processes, and Future Perspectives. *Appl. Microbiol. Biotechnol.* **2019**, *103* (1), 143–157. https://doi.org/10.1007/s00253-018-9483-6.

(41) Huang, Y.; Jing, W.; Zeng, J.; Xue, Y.; Zhang, Y.; Yu, X.; Wei, P.; Zhao, B.; Dong, J. Highly Tough and Biodegradable Poly(Ethylene Glycol)-Based Bioadhesives for Large-Scaled Liver Injury Hemostasis and Tissue Regeneration. *Adv. Healthc. Mater.* **2023**, *12* (27), 2301086. https://doi.org/10.1002/ADHM.202301086.

(42) Vatanpour, V.; Pasaoglu, M. E.; Barzegar, H.; Teber, O. O.; Kaya, R.; Bastug, M.; Khataee, A.; Koyuncu, I. Cellulose Acetate in Fabrication of Polymeric Membranes: A Review. *Chemosphere* **2022**, *295*, 133914. https://doi.org/10.1016/J.CHEMOSPHERE.2022.133914.

(43) Dong, K.; Peng, X.; Wang, Z. L. Fiber/Fabric-Based Piezoelectric and Triboelectric Nanogenerators for Flexible/Stretchable and Wearable Electronics and Artificial Intelligence. *Adv. Mater.* **2020**, *32* (5), 1902549. https://doi.org/10.1002/adma.201902549.

(44) Wang, J. Z.; You, M. L.; Ding, Z. Q.; Ye, W. Bin. A Review of Emerging Bone Tissue Engineering via PEG Conjugated Biodegradable Amphiphilic Copolymers. *Mater. Sci. Eng. C* **2019**, *97*, 1021–1035. https://doi.org/10.1016/J.MSEC.2019.01.057.

(45) Wang, L.; Kou, R.; Shang, Z.; Weng, Z.; Zhu, C.; Zhong, Y. Corona-Enabled Electrostatic Printing for Ultra-Fast Manufacturing of Binder-Free Multifunctional E-Skins. *ACS Appl. Mater. Interfaces* **2021**, *13* (38), 45966–45976. https://doi.org/https://doi.org/10.1021/acsami.1c11386.

(46) Badji, A.; Benseddik, A.; Bensaha, H.; Boukhelifa, A.; Hasrane, I. Design, Technology, and Management of Greenhouse: A Review. *J. Clean. Prod.* **2022**, *373*, 133753. https://doi.org/10.1016/J.JCLEPRO.2022.133753.

(47) Wang, L.; Chiang, W. H.; Loh, K. J. Topological Design of Strain Sensing Nanocomposites. *Sci. Rep.* **2022**, *12* (1), 1. https://doi.org/10.1038/s41598-022-13393-w.

(48) Meng, Q. X.; Xu, W. Y.; Wang, H. L.; Zhuang, X. Y.; Xie, W. C.; Rabczuk, T. DigiSim — An Open Source Software Package for Heterogeneous Material Modeling Based on Digital

Image Processing. *Adv. Eng. Softw.* **2020**, *148*, 102836. https://doi.org/10.1016/J.ADVENGSOFT.2020.102836.

(49) Greenhouse Management. https://www.greenhousemag.com/article/lower-electricity-use-via-natural-ventilation/ (accessed 2024-03-05).

(50) QCSUPPLY. https://www.qcsupply.com/blog/product-tips-and-how-tos/the-importance-of-ventilating-your-greenhouse.html (accessed 2024-03-05).

(51) Costantino, A.; Comba, L.; Sicardi, G.; Bariani, M.; Fabrizio, E. Energy Performance and Climate Control in Mechanically Ventilated Greenhouses: A Dynamic Modelling-Based Assessment and Investigation. *Appl. Energy* **2021**, *288*, 116583. https://doi.org/10.1016/J.APENERGY.2021.116583.

(52) USDA. https://www.nass.usda.gov/Publications/AgCensus/2017/Online_Resources/Census_of_Horticulture_Specialties/index.php (accessed 2024-03-05).

(53) Greenhouse Management. https://www.greenhousemag.com/article/photovoltaic-solar-electricity-for-greenhouses/ (accessed 2024-03-05).

Table of contents (TOC)/Abstract Graphic

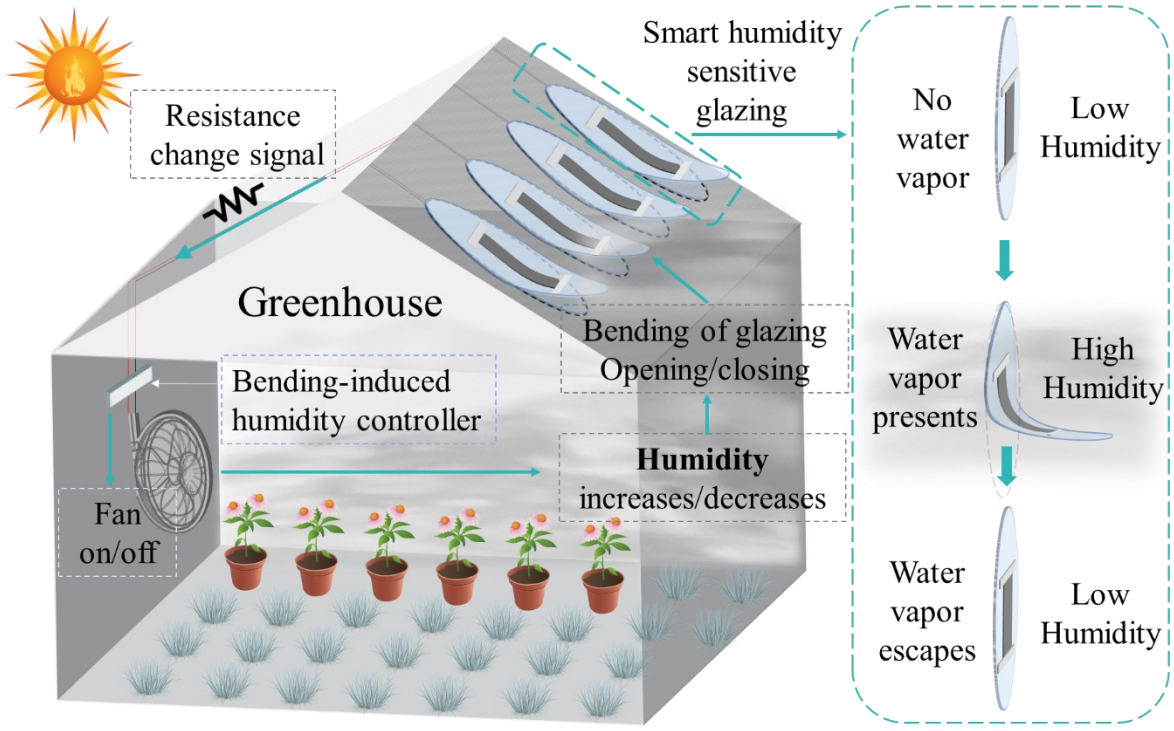

SYNOPSIS

The implementation of eco-friendly and biodegradable smart covers presents a viable alternative to conventional non-degradable coverings for achieving humidity regulation in sustainable greenhouse systems.